# Optomechanical Uncooled Infrared Imaging System: Design, Microfabrication, and Performance

Yang Zhao, Minyao Mao, Roberto Horowitz, Arunava Majumdar, John Varesi, Paul Norton, and John Kitching

***Abstract*—This paper presents the design, fabrication and performance of an uncooled micro-optomechanical infrared (IR) imaging system consisting of a focal-plane array (FPA) containing bi-material cantilever pixels made of silicon nitride (SiNx) and gold (Au), which serve as infrared absorbers and thermomechanical transducers. Based on wave optics, a visible optical readout system is designed to simultaneously measure the deflections of all the cantilever beams in the FPA and project the visible deflection map onto a visible charge-coupled device (CCD) imager. The IR imaging results suggest that the detection resolution of current design is 3–5 K, whereas noise analysis indicates the current resolution to be around 1 K. The noise analysis also shows that the theoretical noise-equivalent temperature difference (NETD) of the system can be below 3 mK. [658]**

***Index Terms*—Focal-plane array (FPA), infrared, interdigited fingers, microcantilever array, microfabrication, optomechanical, uncooled.**

## I. Introduction

INFRARED (IR) vision is a key technology in variety of military and civilian applications ranging from night vision to environmental monitoring, biomedical diagnostics, and thermal probing of active microelectronic devices. By detecting the thermal radiation emitted by a distant object, infrared cameras enable remote sensing, tracking of targets and navigation under visually restricted conditions. For imaging objects near room temperature, IR detectors must be sensitive in the spectral range from 8 to 14 $\mu$m, not only because this is the atmospheric transmission window but also because it contains the peak of the blackbody spectrum for objects at around room temperature. Detectors of IR radiation can be broadly classified into two categories: photonic and thermal. Photonic devices have been made with materials that have energy bandgaps sufficiently small ($E_g \approx 0.1$ eV) to absorb 8–14 $\mu$m IR radiation. However, the small bandgap makes such detectors susceptible to thermal noise, which varies as $\exp(-E_g/k_BT)$, where $T$ is the detector temperature and $k_B$ is the Boltzmann constant. The exponential dependence requires cooling of the detector to cryogenic temperature (about 80 K) to reduce thermal noise. The typical noise-equivalent temperature difference (NETD) for such cryogenic cameras is 5–10 mK. The additional cooling system, however, increases weight and cost and poses reliability problems. This has driven research toward uncooled IR detectors, which rely on photothermal heating due to IR absorption. Such cameras can be classified into two categories, namely: those based on capacitance detections of changes in temperature dependent dielectric constant of pyroelectric materials; and those based on detecting resistance changes in materials having large temperature coefficients of resistivity such as vanadium oxide ($VO_x$) [1]–[4]. Because the thermal noise in such detectors varies as $\sqrt{k_BT}$, cooling to cryogenic temperature does not significantly improve their performance. Hence, they can be usefully operated at room temperature. Kruse *et al.* reported a CMOS integrated $VO_x$ bolometer array with NETD less than 0.1 K [5]. The performance of such uncooled IR cameras has been significantly improved in the recent past with NETD as low as 42 mK for $f/1$ IR lens system with 60 Hz bandwidth [6]. And Raytheon people developed uncooled FPA also based on $VO_x$ microbolometers reaching 25 mK NETD with $f/1$ optics and thermal time constants of 18 ms [7]. Detection in these uncooled cameras is based on electrical signal readout from each pixel. Fabrication complexity of the interconnects on the pixel as well as the readout circuit design has kept the cost prohibitively high for many commercial applications. In addition, because electrical interconnects are used for each pixel, it is difficult to increase the thermal isolation to the radiation limit. Moreover, electronic-based systems such as bolometers are limited inevitably by Johnson noise. This paper presents a different approach to IR vision that uses an uncooled opto-mechanical imaging system. It is shown that because the temperature change is optically detected, thermal isolation can be increased to the radiation limit. In addition, the dominant noise is either thermal vibration or optical readout, which can be controlled externally, thus enabling the NETD to approach the range below 5 mK.

Fig. 1 shows the basic design of this microoptomechanical IR receiver with optical readout (MIRROR) system. At the heart of the system is the focal-plane array (FPA). Each pixel in the array consists of a bimaterial cantilever beam, which bends as its temperature rises due to absorption of the incident infrared radiation. The cantilever deflection is proportional to the change in temperature of the beam and also to the difference between the thermal expansion coefficients of the two cantilever materials. An optical system using visible light simultaneously measures

Manuscript received January 3, 2001; revised August 20, 2001. This work was supported by the DARPA MEMS program under Contract N66001-97-C-8621. Subject Editor N. de Rooij

Y. Zhao, M. Mao, R. Horowitz, and A. Majumdar are with the Department of Mechanical Engineering, University of California, Berkeley, CA 94720 USA (e-mail: majumdar@me.berkeley.edu.)

M. Mao is currently with the Optical Coating Laboratory Inc., Santa Rosa, CA 95407 USA.

J. Varesi is with the Santa Barbara Research Center (Raytheon), Goleta, CA 93117 USA.

P. Norton is with the IR Vision, Santa Barbara, CA 93105 USA.

J. Kitching is with the Time and Frequency Division, The National Institute of Standards and Technology-Boulder, Boulder, CO 80305 USA and also with JILA, the University of Colorado, Boulder, CO 80309-0440 USA.

Publisher Item Identifier S 1057-7157(02)02343-0.

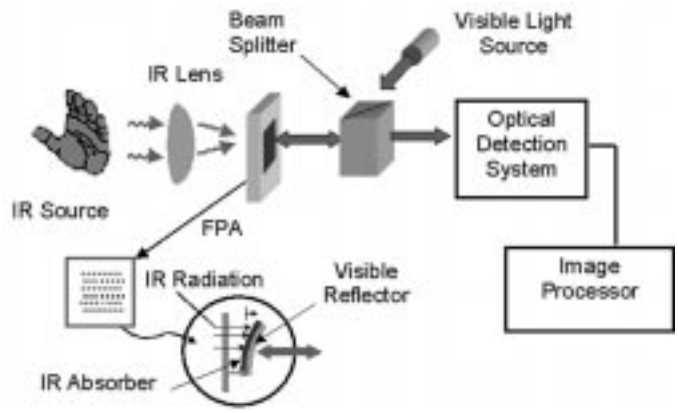


Fig. 1. Schematic diagram of the uncooled optomechanical infrared imaging system.

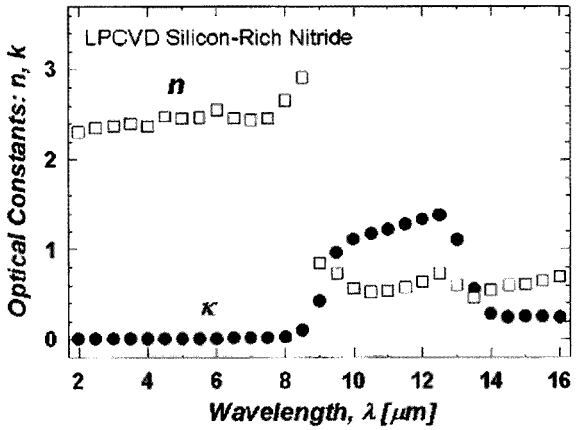


Fig. 2. Real $(n)$ and imaginary $(k)$ parts of the refractive index of an LPCVD $SiN_x$ thin film.

the deflections of all the cantilevers of the FPA, and collectively projects a visible image of the spatially varying IR radiation onto a visible charge-coupled device (CCD) or CMOS array.

As will be shown in this paper, the attractive features of the MIRROR system are as follows:

a) uncooled operation is possible since the noise does not exponentially depend on temperature;
b) direct-view optical readout eliminates the need for electrical interconnects to each pixel and scanning electronics, thus reducing fabrication complexity and costs;
c) the optical readout eliminates metal on the legs and thus enables the thermal isolation of each pixel to approach the radiation limit;
d) the power dissipation for optical readout is much less than for electrical measurement methods, thus simplifying power and thermal management.

The use of the single bimaterial microcantilever for sensing of temperature [8] and radiation has been demonstrated by several groups [9]–[14]. Based on this, Manalis *et al.* [15] made the first attempt to build a camera by fabricating an FPA of Si/Al bimaterial cantilevers which they used to detect absorption of an IR laser operating at 0.78 $\mu$m wavelength. However, Si and Al are not suitable for IR detection in the 8–14 $\mu$m range due to their lack of IR absorption in this wavelength range and their high thermal conductivity. Previous work in the author's group on the MIRROR system with single-layer bimaterial structures showed the first thermal IR images [16], [17]. In Section II, the paper presents a detailed description of the design procedure including thermal and thermomechanical behavior of the pixel as well as the optical system design. Analysis of noise and system performance in Section V shows the NETD of the present system to be 2 K. The calculation in Section V also shows that the theoretical limit of the system can reach a resolution better than 5 mK.

## II. Design

The design of a focal-plane array should maximize the pixel's temperature rise and optimize the thermomechanical response for a given incident flux of IR under the constraints of predetermined pixel size. In addition, the fill factor should also be maximized. The thermal time constant of the pixel should be compatible with the frame rate of CCD system to achieve real-time detection. To optimize the system performance, material selection, thermal design, thermomechanics, and IR as well as visible optics are important issues that need to be considered concurrently.

TABLE I
Thermophysical Properties of $SiN_x$, Si, Au, and Al

| | Density $\rho$ x $10^{-3}$ kg/m$^3$ | Young's Modulu $E$ GN/m$^2$ | Thermal Cond., $k$ W/(m·K) | Expansion Coeff., $\alpha$ [x $10^{-6}$ K$^{-1}$] | Heat Capacity $c$, J/kg·K |
|---|---|---|---|---|---|
| $SiN_x$ | 2.40 | 180 | 5.5±0.5 | 0.8 | 691 |
| Si | 2.33 | 100 | 135 | 2.6 | 700 |
| Au | 19.30 | 73 | 296 | 14.2 | 129 |
| Al | 2.70 | 80 | 237 | 23.6 | 908 |

### A. Materials

The two materials selected for IR absorbing bi-material cantilevers should meet following basic requirements:

a) one of the materials must absorb IR in the range of 8–14 $\mu$m, and the other a good reflector in the visible spectrum to be suitable for optical readout;
b) the two materials must have a large mismatch in thermal expansion coefficients;
c) the materials must be compatible with microfabrication processes;
d) the films of the materials must have low residual stress;
e) materials should be possess good chemical inertness;
f) the thermal conductivity of at least one of the two materials must be low.

In this work, low-pressure chemical vapor deposited (LPCVD) low-stress silicon nitride ($SiN_x$) and gold (Au) were used in the bi-material cantilever. Figure 2 shows the the real $(n)$ and imaginary $(k)$ parts of the refractive index of $SiN_x$, indicating the absorption peak in the 8–14 $\mu$m spectral range. Since $k \approx 1$, the optical penetration depth, $l = \lambda_{\rm IR}/4\pi k$, is about 1 $\mu$m in this spectral range. The thermal conductivity of low-stress LPCVD silicon nitride used here was measured by the $3\omega$ method [18]. Table I provides the properties of $SiN_x$ and Au as well as those of Si and Al for comparison. $SiN_x$ and Au show the desirable large mismatch in expansion coefficient. In addition, low-stress

nitride also has low thermal conductivity, which is critical for designing thermal isolation.

It is well known that polymers have thermal conductivities typically in the range of 0.1–0.5 W/(m·K) and expansion coefficients in the range of $(0.5\text{–}1) \times 10^{-4}$ K$^{-1}$, making them ideal materials for thermomechanical IR detector. However, we found that the inherent stresses in the polymer films were too high to make the cantilevers usable. Hence, we selected $SiN_x$ and Au as the cantilever materials.

### B. Thermal Design

Consider a pixel in the FPA initially at thermally equilibrium with the surroundings. The temperature change in the cantilever $\Delta T_c$ due to the temperature change of the target IR source $\Delta T_s$ can be expressed as [2]

$$H = \frac{\Delta T_c}{\Delta T_s} = \frac{A_{ab}\varepsilon\tau_o\pi(dP/dT_t)}{4F_{\text{no}}^2(G_{\text{leg}} + G_{\text{rad}})}. \tag{1}$$

Here $F_{\text{no}}$ is the $f/\#$ of the IR imaging lens $(=1)$, $A_{ab}$ the pixel absorption area, $\varepsilon$ the emissivity of the pixel $(=0.8)$, $\tau_o$ the transmissivity of the IR optical head $(=0.9)$, and $(dP/dT_t)$ is the fraction of the radiative energy emitted by the target source at temperature $T_t$ ($\sim$300 K). Within the 8–14 $\mu$m spectral band $dP/dT_t = 0.63$ W/m$^2$-sr-K. Here, $G_{\text{leg}}$ is the thermal conductance of the thermal isolation leg and $G_{\text{rad}}$ the radiation conductance of the pixel, which follows:

$$G_{\text{rad}} = 4A_{\text{pixel}}\left(\varepsilon_{\text{Au}} + \varepsilon_{\text{SiN}_x}\right)\sigma T^3, \tag{2}$$

where $A_{\text{pixel}}$ is the total pixel area, $\sigma$ the Boltzmann constant, and $T$ the pixel temperature ($\sim$300 K). The emissivities of gold and $SiN_x$ are 0.01 and 0.8, respectively. The leg's conductance can be expressed as

$$G_{\text{leg}} = A_{\text{leg}}k/L_{\text{leg}} \tag{3}$$

where $A_{\text{leg}}$ is the cross-sectional area of the leg, $k$ the thermal conductivity of the leg material and $L_{\text{leg}}$ the total length of the leg.

The radiative conductance is the intrinsic conductance of the cantilever since the radiative emission is related directly to the absorption through Kirchoff's law. To reach the radiative conductance limit for the total conductance, the leg's conductance $G_{\text{leg}}$ must be lowered below the radiative conductance. According to Eq. (3), to reach a small enough thermal conductance, it is important to choose a material of low thermal conductivity and to design the supporting leg structure of the cantilever with large length and small cross-sectional area. It is clear that Au is an ideal material, due to its high thermal expansion coefficient and its high reflectivity in the visible range. However, because Au is thermally conductive, it is imperative that each pixel must consist of two regions—1) a metallized Au/$SiN_x$ bi-material region that produces the cantilever deflection due to temperature change; and 2) an unmetallized leg that thermally isolates the bi-material region from the substrate. The unmetallized region could be made of $SiN_x$ or another material of lower thermal conductivity.

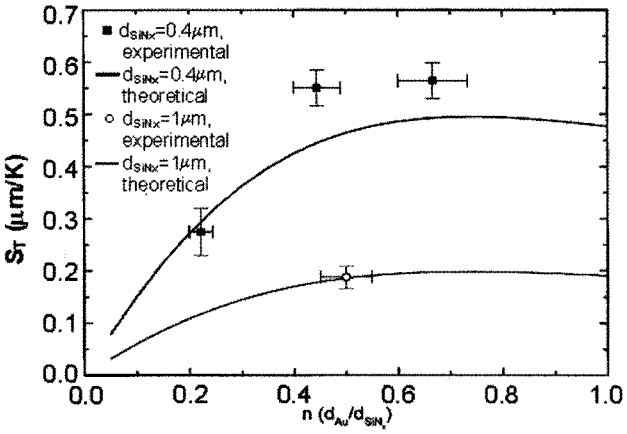


Fig. 3. Experimental data and theoretical prediction of the temperature sensitivity of bi-material cantilever deflection, $S_T$, as a function of thickness ratio $n(d_{\text{Au}}/d_{\text{SiN}_x})$.

### C. Thermomechanical Design

To determine the deflection of the cantilever as a function of temperature rise, one must solve the thermomechanical governing equation for a bi-material cantilever beam, which is given as [9], [12]

$$\frac{d^2z}{dx^2} = 6(\alpha_{\text{Au}} - \alpha_{\text{SiN}})\left(\frac{d_{\text{Au}} + d_{\text{SiN}}}{d_{\text{SiN}}^2 K}\right)\Delta T$$
$$z = 0; \quad \frac{dz}{dx} = 0 \quad \text{at } x = 0, \tag{4}$$

where $d$ is the cantilever thickness, $\alpha$ the thermal expansion coefficient, $z$ the cantilever deflection at a distance $x$, and $\Delta T$ the temperature rise of the cantilever. Here $x = 0$ is where the metallization starts and $L_m$ the length of the metallized cantilever. $K$ is a structure parameter given as

$$K = 4 + 6n + 4n^2 + \phi n^3 + \frac{1}{\phi n};$$
$$n = \frac{d_{\text{Au}}}{d_{\text{SiN}}}; \quad \phi = \frac{E_{\text{Au}}}{E_{\text{SiN}}} \tag{5}$$

where $E$ is the elastic modulus. Equation (4) can be solved and the thermomechanical sensitivity, $S_T = \delta/\Delta T$ of the cantilever can be found to be

$$S_T = \frac{\delta}{\Delta T} = 3(\alpha_{\text{Au}} - \alpha_{\text{SiN}})\left(\frac{n+1}{K}\right)\left(\frac{L_m^2}{d_{\text{SiN}}}\right) \tag{6}$$

in which $\delta$ is the deflection of the cantilever at $x = L_m$. It is clear from Eq. (6) that the mismatch in thermal expansion must be large. The optimum value of $n$ depends on $E_{\text{Au}}/E_{\text{SiN}}$, which is theoretically predicted to be $n_{\text{opt}} = 0.75$. Fig. 3 shows reasonable agreement between the predicted and the experimentally obtained values of $S_T$ as a function of $n$ for two different thickness of the $SiN_x$ film. Equation (6) also indicates that the length must be maximized and the cantilever thickness must be reduced.

For the temporal response of the thermal imaging system to be compatible with real-time visible imagers ($\sim$30 frames/sec), the thermal time constant $\tau$ of the pixel must lie between 10 and

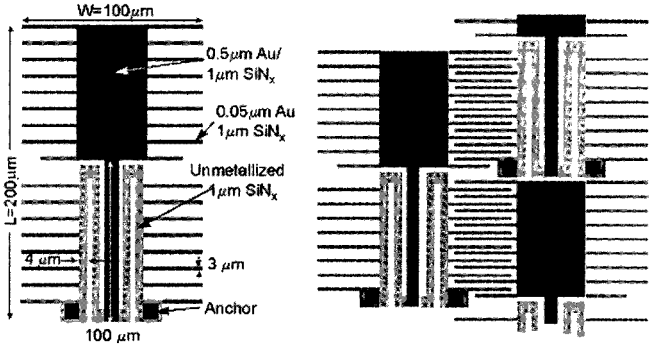


Fig. 4. Details of pixel tilting design.

20 ms. $\tau$ is determined by the pixel's heat capacitance $C_{\rm th}$, and thermal conductance $(G_{\rm leg} + G_{\rm rad})$:

$$\tau = C_{\rm th}/(G_{\rm leg} + G_{\rm rad}) \tag{7}$$

where $C_{\rm th} = \sum_i (\rho A d C)_i$, $\rho$ is the material density, $A$ the area of each cantilever element, $d$ the thickness, and $C$ the material heat capacity, and $i$ indicates each material used in the pixel.

### *D. Pixel Tiling*

Based on the above design analysis, Fig. 4 shows the pixel design as well as the pixel tiling layout that was adopted for the FPA. A staggered tiling of the pixels allowed doubling of the cantilever length (200 $\mu$m) for the pixel size (100 $\mu$m$\times$100 $\mu$m). Between the anchors and the metallized region of the cantilever were two legs whose lengths totaled 200 $\mu$m with 1 $\mu$m thickness. Table II lists the thermal and mechanical parameters of this design. Notice that the leg's conductance is higher than the radiative limit by a factor of 5. The interdigitated fingers between two adjacent pixels were used as a deformable diffraction grating for optically detecting cantilever deflections (see details later). There are two sets of interdigitated fingers on each pixel. One set is on the metallized region, and the other on the thermal isolation leg. With pixel tilling arrangement, the fingers on the metallized region were meshed with those on the legs of the adjacent pixels. Since the legs were unmetallized and did not deform due to temperature rise, the relative displacement of the diffraction grating was thus maximized.

### *E. Optical Readout Design*

An optical readout is a data-acquisition method that measures each pixel's deflection optically as opposed to electronically. The goal of the optical readout is to simultaneously measure deflections of all pixels with sub-nanometer resolution and to display onto a human eye or a visible CCD/CMOS imager an intensity map based on the collective deflections. The key point is to collect signals from the whole array simultaneously instead of scanning each pixel one by one, and still keep high sensitivity with negligible crosstalk; that is, the pixel's signal should be independent of its neighbor's signal.

The deflection of each bi-material cantilever induced by temperature change can be resolved into a vertical displacement and a change in slope. Correspondingly, there are two basic strategies for measuring a cantilever's deflection: (i) beam steering based on the change in slope; and (ii) various interference and diffraction methods based on the change in vertical displacement. A change in cantilever slope will steer an incident optical beam, thus translating it across a plane. For the case of single cantilevers, a single position-sensitive photodiode located far away from the cantilever, as used in the atomic force microscope (AFM), can measure the translation of the reflected beam. This leads to measurement of cantilever deflection with sub-Angstrom resolution [19]. However, when attempting to measure deflection of an array of cantilever beams, the light reflected from the micron-size cantilever surfaces is strongly diffracted and overlapped, thus producing cross talk. This diffraction effect constrains the measurement plane to be very close to the FPA, in which case the required resolution of deflection is difficult to achieve by beam-steering methods. Therefore, the optical readout systems we have developed are based only on the vertical change in position of the cantilever beams. Here, we focus on the readout schemes based on intensity changes resulting from the deformable diffraction gratings.

When coherent light is incident on a diffraction grating, the diffracted light forms a spatial Fourier transform of the grating in the far field [20]. This can be achieved with a collimated laser beam and a focusing lens, as shown in Fig. 5. The spatial Fourier transform pattern consists of the zeroth-, first- and higher-order peaks. From Helmholtz-Kirchoff diffraction analysis [21], we know that each order of the diffraction signal from the deformable grating varies from minimum to maximum in response of the vertical displacement of $\lambda_{\rm vis}/4$ of fingers. Therefore, in principle each order can be used to detect cantilever deflection. The important thing is to filter out the other orders and look only at a single order. In the previous work [16], [17], a pinhole array mounted on the FPA chip served as a spatial filter in real space to transmit only the zeroth order. Another option is to filter in $K$-space (or frequency space).

The setup for the readout system using the first order of diffraction is shown schematically in Fig. 5. The entire FPA was illuminated by a collimated laser beam. The cantilever array with diffraction grating generated the diffracted light at specific angles corresponding to the order of diffraction, and the energy distribution among the diffraction orders depended on the relative distance between the movable and fixed interdigital fingers. The first focusing lens performed a Fourier transform and converted the collimated light at different diffracted angles to a series of independent spots at the focal plane. The spatial filter at the focal plane allows only the first order to pass through. It should be noted that the spatial separation of the 0th, 1st, and 2nd order on the Fourier plane corresponds to the periodicity of the interdigital fingers. The pixel-to-pixel periodicity produced sub-order peaks within each of the main orders, as can be seen in Fig. 5. Hence, the information of the whole array is contained within each peak. The second focusing lens performed an inverse Fourier transform and reconstructed the image of the cantilever array from only the first-order diffracted light. The intensity of the final image depended only on the energy distribution of first-order diffracted light generated from the correponding cantilevers. By an analysis

TABLE II
SINGLE-LAYER FPA DESIGN PARAMETERS

| Pixel Size (μm) | $L_m$ (μm) | $L_{leg}$ (μm) | $G_{leg}$ (W/K) | $G_{rad}$ (W/K) | $H$ | $S_T$ (μm/K) | $\omega_0$ (rad$^{-1}$) | $\tau$ (ms) | $g$ (N/m) |
|---|---|---|---|---|---|---|---|---|---|
| 100 | 200 | 200 | $1.1\times10^{-7}$ | $3.5\times10^{-8}$ | 0.03 | 0.11 | $1.3\times10^{4}$ | 80 | $1.1\times10^{-2}$ |

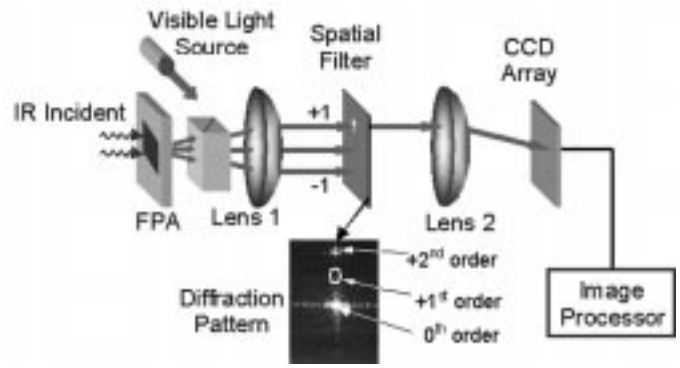


Fig. 5. Schematic diagram of the optical setup for IR imaging using first-order diffraction. Lens 1 performs a Fourier transform of the optical signal reflected of the FPA. The zeroth-, first-, and second-order diffraction peaks can be observed on the Fourier plane. Lens 2 performs an inverse Fourier transform of the first-order signal and reconstructs the signal on the CCD imager.

using Fraunhofer diffraction theory [20], one can derive the diffraction intensity of each cantilever in the image plane to be

$$I = I_0 \cos^2(2\pi h(x_i, y_i)/\lambda_{\text{vis}}) \tag{8}$$

where $h(x_i, y_i)$ is the distance between the movable and fixed fingers of the cantilevers at a location $(x_i, y_i)$ on the FPA, $I_0$ the normalized intensity of the 1st order diffraction peak, $\lambda_{\text{vis}}$ the wavelength of the visible illumination laser and $I(x_i, y_i)$ the intensity on the image plane $(x_i, y_i)$. Details of this technique have been described elsewhere [22].

An analog monochrome CCD camera and an 8-bit image processor captured the reconstructed visible image. Before the FPA was exposed to the IR source, the background image was captured and stored in the image processor. The background intensity of each pixel corresponded to the initial deflection of the diffraction grating $(h_0)$ and can be expressed as

$$I_b = I_0 \cos^2(2\pi h_0(x_i, y_i)/\lambda) \tag{9}$$

The thermal image was grabbed after the FPA was exposed to the IR source, and can be written as

$$I_t = I_0 \cos^2[2\pi(h_0(x_i, y_i) + \delta(x_i, y_i))/\lambda] \tag{10}$$

where $\delta$ is the pixel's deflection due to the IR absorption.

The image processor performed a real-time subtraction between the images captured before and after the IR exposure to provide an offset subtraction and correction for nonuniformity. The intensity distribution of the final image is

$$I = I_t - I_b = I_0 \lfloor \cos^2(2\pi(h_0(x_i, y_i) + \delta(x_i, y_i))/\lambda) - \cos^2(2\pi h_0(x_i, y_i)/\lambda) \rfloor \tag{11}$$

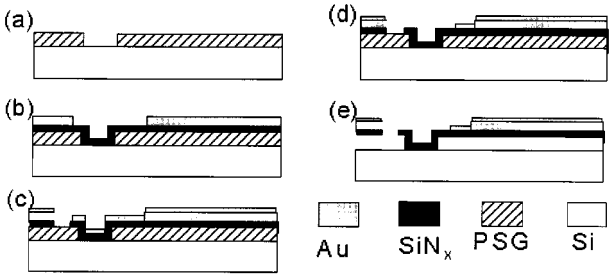


Fig. 6. Microfabrication process sequence of FPA. (a) Deposition of PSG and anchor pattern. (b) Deposition of $SiN_x$ followed by deposition of thick Au Layer; pattern the thick Au layer. (c) Deposition of thin Au layer and cantilever pattern. (d) Removal of the Au from the thermal isolation leg. (e) Removal of PSG and release of the cantilever.

Notice that the initial deflection of the cantilever plays an important role in the image intensity change for each pixel, since the relationship between the intensity $I$ and deflection $\delta$ is not linear. The optomechanical sensitivity, $\beta = (dI/d\delta)/I_0$, of a pixel depends therefore on the initial deflection $h_0$.

## III. MICROFABRICATION

The FPA's containing $50 \times 70$ pixels were fabricated using surface micromachining technology. The process consisted typically of four masking steps—anchor patterning, thick-metal patterning, cantilever definition and thin-metal patterning, as shown schematically in Fig. 6.

The process started with a boron-doped silicon wafer with resistivity of 10 to 20 ($\Omega$·cm). The first step was deposition of a phosphorous silicate glass (PSG) film 5 $\mu$m thick and anchor patterning to form the desired gap between the cantilever and the substrate. Second, a low stress LPCVD silicon nitride film 1 $\mu$m thick was deposited and followed by thermal evaporation of a gold film 0.5 $\mu$m thick on top to form the bimaterial structure. A layer of chrome 10 nm thick was used to promote adhesion between the gold and the nitride film. The thick gold film was removed from the regions where the thermal resistance beams (legs) and diffraction-grating finger structures (combs) were to be formed later. Third, a layer of gold 50 nm thick was evaporated, and then the cantilever patterns were defined. The fourth step was to remove the unwanted gold layer on the thermal resistance beams. Finally, the PSG sacrificial layer was etched away in HF to release the cantilevers, and the FPA was dried by critical-point drying to prevent the cantilever from sticking to the substrate.

Fig. 7(a) shows an electron micrograph of typical Au/$SiN_x$ bimaterial cantilevers with a length of 200 $\mu$m and diffraction grating finger width of 3 $\mu$m. It was observed that the cantilever was slightly bent away from the Si substrate, and the initial bending at the end of the cantilever, as measured by the dis-

(a)

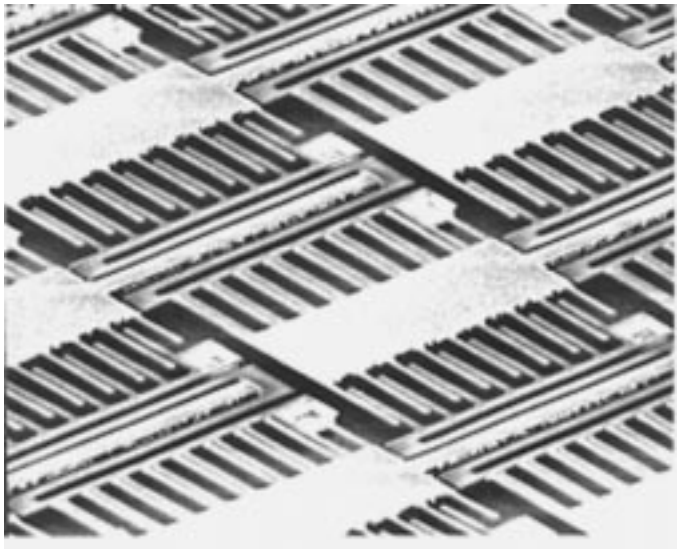

(b)

Fig. 7. Scanned electron micrograph (SEM) pictures of pixels: (a) Au (0.5 $\mu$m)/SiN$_x$ (1 $\mu$m) cantilevers, (b) bare SiN$_x$ cantilevers.

placement from its original position at room temperature, was about 10 $\mu$m. This bending was caused by residual stress in the thin films, which included the intrinsic stress gradient across the SiN$_x$ and Au films, as well as the thermal stress between these two films due to mismatch in thermal expansion.

The initial bending of the cantilever strongly influences the performance of the optical readout system and, hence, its reduction is currently a major research effort. It is well known that the residual tensile stress in LPCVD SiN$_x$ film depends strongly on the deposition conditions such as temperature, pressure and the ratio of the flow rate of source gases during deposition. We used dichloric silane (DCS) and ammonia (NH$_3$) as sources of silicon and nitrogen in LPCVD deposition. By increasing the flow ratio of DCS/NH$_3$ $= 6:1$, we could get almost flat cantilevers of bare silicon nitride. Fig. 7(b) shows the SEM picture of released cantilevers of bare silicon nitride with initial bending of about 4 to 5 $\mu$m at the end of the 200 $\mu$m length. Further reduction in bending would be difficult.

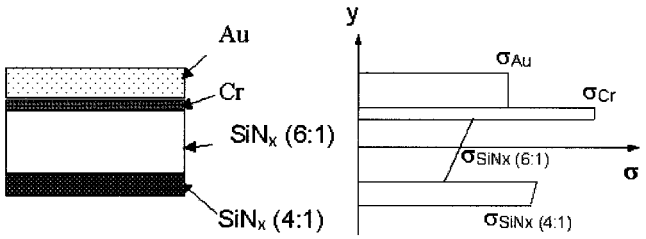


Fig. 8. Schematic diagram of residual stresses in the different layers of the cantilever showing the approach to balancing the high tensile stress of Cr and Au films with an additional 4:1 SiN$_x$ film on the opposing side.

By comparing the initial bending of cantilevers with and without the metal films [see Fig. 7(a) and (b)], we noted that the initial bending of cantilever caused by metallization was significant. Hence, it was also important to reduce the tensile stress caused by metal deposition. We found that the thin Cr adhesion layer and the thick gold film contributed almost equally to the stress. In principle, the stress caused by metallization can be reduced by controlling the temperature and rate of deposition, but it was found to be very difficult to eliminate the stress completely.

In general, the bending of a cantilever beam resulted from the stress gradient across the film's thickness. Bending of cantilever away from the substrate indicates that the top of the beam has higher tensile stress than that of the bottom. In principle, we can reduce bending by reducing this gradient. However, we found it was extremely difficult to completely eliminate this stress gradient. Therefore, we used another approach. The schematic diagram of stress balance is shown in Fig. 8. Based on the fact that the residual tensile stress of SiN$_x$ deposited at low DCS/NH$_3$ ratio $r$ is much higher than that at high ratio [23], we used SiN$_x$ film deposited at $r = 4$ as a high-stress layer on the bottom of the cantilever, that is, on the side opposite to the metal film. Our experiment showed that by using a layer of SiN$_x$ of $r = 4$ and 0.1 $\mu$m thick at the bottom of a SiN$_x$ of $r = 6$ and 1 $\mu$m thick, it was possible to effectively adjust a cantilever 200 $\mu$m long from bending up by 4–5 $\mu$m to bending down by 15 $\mu$m. For metallized cantilevers, in principle, proper choice of the thickness ratio of the SiN$_x$ layer of $r = 4$ to that of $r = 6$ and the metal layers can lead to flat cantilevers. However, due to the poor reproducibility of the stress controlling during Au/Cr metal deposition, it is difficult to precisely predict the thickness of the stress balance layer in order to produce flat cantilevers. Therefore, it is necessary to make the optical readout technique sufficiently robust to account for initial deflections.

We found that the temperature sensitivity $S_T$ of the Au/SiN$_x$ cantilever depended strongly on the adhesion layer. With too thin or no adhesion layer, a poor bimaterial effect was observed. Only when the Cr adhesion layer had thickness $>7$ nm was a high and reproducible $S_T$ obtained. Therefore, we used a Cr film 7–10 nm thick as the adhesion layer in this work.

## IV. Imaging Results

Fig. 9 shows a thermal image of a human hand, where the image was made by first-order diffraction with an $f/1$ IR lens. In the image, there appear to be some pixels that are not as bright as others. This was due most likely to nonuniformities in

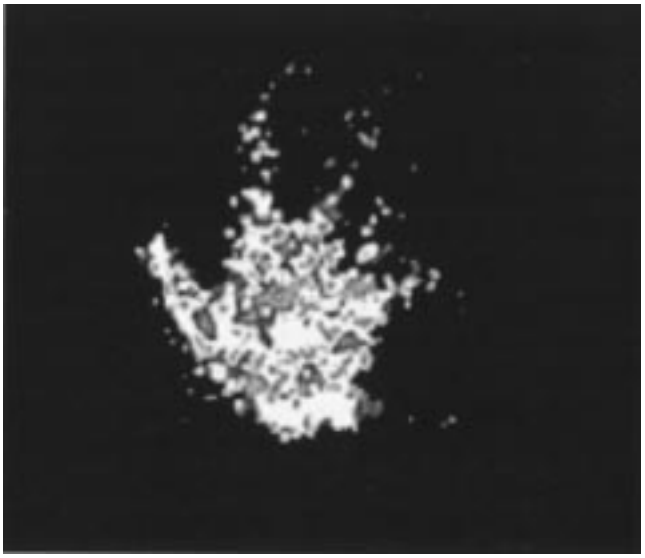

Fig. 9. Thermal image of a human hand using first-order diffraction optics with $f/1$ IR lens.

the pixels and the linear subtraction algorithm described in Eq. (11). The lowest IR source temperature at which infrared images could be observed was about 30 °C with the background temperature around 25 °C. Due to pixel nonuniformity it is difficult to estimate a noise-equivalent temperature difference (NETD) for the system. The best pixels exhibited NETD in the range of 2 to 5 K for the present design.

As a preliminary test, the temperature of the entire FPA was varied to study the optical readout method. Raising the FPA's temperature would reduce the initial upward cantilever deflection and therefore influence the optical diffraction. The performance improved if the initial bending of the cantilevers was close to zero, thus making it necessary to heat the FPA above room temperature. In our experiments the optimum operating temperature was between 35 and 85 °C, which depended on the initial deflection of the cantilevers after fabrication.

## V. Noise Analyses

Noise-equivalent temperature difference (NETD) defines the performance of an infrared imaging system. NETD is the equivalent temperature change in an IR source that can be detected with a signal-to-noise ratio of unity. The NETD of the system is determined by the total noise level in the system. Therefore, it is important to examine all the possible noise sources in the system.

### A. Thermodynamic Fluctuation Noise

Based on the statistical nature of the heat exchange with the environment, any thermodynamic system exhibits random fluctuations in temperature, known as thermodynamic fluctuation noise. For the cantilever pixel, the mean square temperature fluctuation at low frequency range is [1]:

$$\Delta T_{\rm th} = \sqrt{4k_B T^2 B/G_{\rm total}} \tag{12}$$

where $G_{\rm total}$ is the total thermal conductance from the cantilever to environment, $k_B$ Boltzmann's constant, $B$ the detection bandwidth (=30 Hz) and $T$ the cantilever's temperature.

### B. Vibration Noise

Vibration noise arises from two sources: thermal and external. Thermomechanical vibration in a mechanical system comes from $k_BT$ thermal energy and is fundamental in nature. The noise at off-resonant frequencies can be calculated as [19]

$$\delta_{\rm th,vib} = \sqrt{(4k_B T\Delta f)/(g\omega_o Q)} \tag{13}$$

where $\Delta f$ is the measurement bandwidth, which is typically about 30 Hz for a CCD detector; $Q$ the resonance quality factor, which is the ratio of the vibration amplitude at resonant frequency to that at off-resonant frequency; and $Q$ is typically about 10 at atmospheric pressure, and 100–1000 in vacuum. Also, $g$ is the cantilever's spring constant and $\omega_o$ the system resonant frequency. Using the thermomechanical response $S_T$ of the cantilever, thermomechanical noise can be converted to an equivalent temperature fluctuation as

$$\Delta T_{\rm th,vib} = \delta_{\rm th,vib}/S_T. \tag{14}$$

Notice that the thermal vibration noise is also related to the cantilever's spring constant and the resonant frequency. Hence, by carefully designing the cantilever spring constant $g$, this vibration noise can be controlled to be smaller than the temperature-fluctuation noise $\Delta T_{\rm th}$.

Any optical detection method using interference will suffer external environmental vibration. Generally this noise is suppressed effectively by a mechanical isolation system such as an optical table.

### C. Temperature Stability

To control the temperature of the FPA, a temperature sensor and thermoelectric cooler were used in a feedback control circuit. The FPA was mounted on a copper ring, which was then mounted on four thermoelectric coolers. The temperature sensor measured the temperature of the copper ring as the feedback signal to the control system. The temperature fluctuation at the substrate was defined by the resolution of the temperature-control system at $\Delta T_{\rm sub} = 20$ mK. Thus the temperature fluctuation on the cantilever induced by it is [16]

$$\Delta T_{\rm tc} = \Delta T_{\rm sub}/(1 + G_{\rm rad}/G_{\rm leg}) \tag{15}$$

### D. Optical Readout Noise

The optomechanical sensitivity is defined as $\beta = (\delta I/\delta h)/I_0$. According to Eq. (10), $\beta$ has a maximum value of $\beta_{\rm max} = 4\pi/\lambda_{\rm vis} = 16.1\ \mu{\rm m}^{-1}$ for a He-Ne laser at $\lambda_{\rm vis} = 683$ nm.

The noise in the optical readout system originates in both the CCD and the laser. Dark current in the CCD is generated via a random process and therefore adds noise to the measurement of pixel illumination. Since the dark current is small compared to the current generated by the light, the noise component is small. In addition, the digitization of the CCD output voltage

TABLE III
NOISE ANALYSIS FOR SINGLE-LAYER FPA DESIGN

| $\Delta T_{th}$ (μK) | $\Delta T_{th,vib}$ (μK) | $\Delta T_{CCD}$ (mK) | $\Delta T_{laser}$ (mK) | $\Delta T_{sub}$ (mK) | $\Delta T_{total}$ (mK) |
|---|---|---|---|---|---|
| 32 | 52.6 | 2 | 0.18 | 17 | 17 |

adds noise to the signal. For an 8-bit digitizer, the error is of order $1/256 = 0.004$. The laser adds noise through fluctuations of the intensity incident on the FPA. Laser noise can be minimized through an appropriate choice of laser or using stabilization feedback techniques. Finally, the lowest limit of shot noise in the detection process contributes noise equal to $1/\sqrt{N}$, where $N$ is the full-well capacity of the CCD pixels. For the monochrome interline transfer CCD camera used in the experiment (full-well capacity of $6 \times 10^4$ electrons) the shot noise results in a $dI/I$ equal to roughly 0.004. With the optical detection system sensitivity $\beta$ and the thermomechanical response of the cantilever $S_T$, the CCD noise can be converted to an equivalent temperature noise on the cantilever according to

$$\Delta T_{\rm CCD} = (\Delta I/I)_{\rm CCD}/S_T\beta. \tag{16}$$

In addition to the CCD, the laser also produces noise due to changes in cavity resonance and various other factors. For a 5 mW cylindrical He-Ne laser with output wavelength 632.8 nm, at 30 Hz bandwidth, the noise amplitude $\Delta I/I \cong 3 \times 10^{-4}$ according to our calibration. Converting it to temperature noise we have

$$\Delta T_{\rm laser} = (\Delta I/I)_{\rm laser}/S_T\beta. \tag{17}$$

### *E. Total Noise*

The total noise that is expressed as temperature fluctuation is the statistical average of all the noises mentioned above. Assuming that these are statistically uncorrelated, the total noise can be expressed as

$$\Delta T_{\rm total} = \sqrt{\sum \Delta T_i^2}. \tag{18}$$

For the pixels and the optical readout system described earlier, Table III lists noise levels from each source, and the total noise is equal to 17 mK.

Using $\Delta T_{\rm total} = 17$ mK for our system, the NETD can be estimated from the cantilever's temperature-transfer function $H$ as

$$\text{NETD} = \Delta T_{\rm total}/H = 1.1 \text{ K} \tag{19}$$

where $H = 0.03$ as indicated in Table II.

Notice that in this case the substrate's temperature-fluctuation noise is at present the dominant noise for the present technology. However, the thermodynamic temperature fluctuation noise is the intrinsic noise for all the uncooled IR system since it is related only to the thermal mass of the structure and cannot be externally controlled. Hence, the temperature fluctuation noise limited $\text{NETD}_{\rm TF}$ is regarded the fundamental thermal detection limit of the system:

$$\text{NETD}_{\rm TF} = \Delta T_{\rm th}/H = 1.1 \text{ mK}. \tag{20}$$

Since value of $H$ strongly affects the detection limit and $H$ is inversely proportional to thermal conductance $G$ as indicated in (1), a good thermal isolation is important in lowering the system NETD. Comparing system NETD with $\text{NETD}_{\rm TF}$, it is evident that the NETD can potentially be improved by a factor of 1000 if one can reduce the level of other noise sources to be below $\Delta T_{\rm th}$. The following discussion shows the possibility in approaching this limit in the MIRROR system.

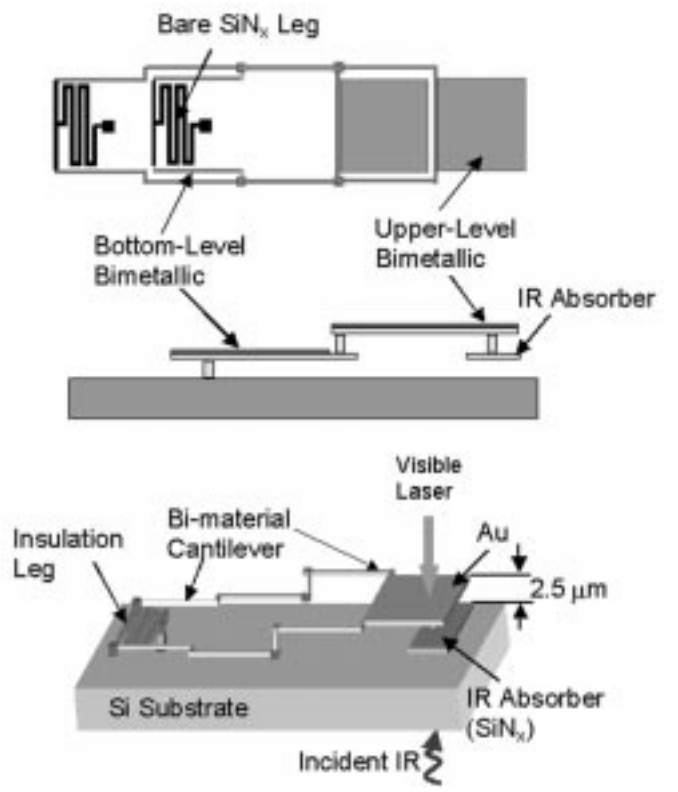


Fig. 10. Details of the proposed two-layer pixel geometry containing a thermal-isolation leg, a thermally isolated Au/$SiN_x$ bimaterial cantilevers, and an IR absorber.

## VI. PERFORMANCE LIMITS AND FUTURE WORK

To improve the system performance and increase the detection resolution, several design issues must be considered, namely, IR, thermomechanical, optical designs, and system stability.

To increase pixel response, we propose a two-layer design of the FPA as shown in Fig. 10. The bottom layer contains the thermal isolation leg, bottom-level bimaterial cantilever and an

TABLE IV
TWO-LAYER FPA DESIGN PARAMETERS

| Pixel Size (μm) | $L_m$ (μm) | $L_{leg}$ (μm) | $A_{abs}$ ($\mu m^2$) | $G_{leg}$ (W/K) | $G_{rad}$ (W/K) | $H$ | $S_T$ (μm/K) | $g$ (N/m) |
|---|---|---|---|---|---|---|---|---|
| 25 | 90 | 50 | 320 | $6\times10^{-8}$ | $1.4\times10^{-10}$ | 0.002 | 0.12 | $6.2\times10^{-2}$ |
| 65 | 240 | 100 | 1710 | $3\times10^{-8}$ | $1.1\times10^{-8}$ | 0.03 | 0.88 | $3.2\times10^{-3}$ |
| 110 | 400 | 100 | 7600 | $3\times10^{-8}$ | $4.5\times10^{-8}$ | 0.06 | 2.5 | $6.8\times10^{-4}$ |

IR absorption pad. The top layer contains the upper-level bimaterial cantilever and a gold reflector for visible optical detection. In this design, the bimaterial cantilever's length $L_m$ is four times the pixel size. Hence, the design provides larger $S_T$ ($S_T \sim L_m^2$), and at the same time has higher spatial resolution compared to the one discussed above. As shown in Eq. (6): $S_T \sim 1/d_{\mathrm{SiN}_x}$. Therefore, the sensitivity can be increased by thinning the $\mathrm{SiN}_x$ film. Considering the uniformity of microfabrication, the minimum thickness of $\mathrm{SiN}_x$ layer should be approximately 0.2 $\mu$m. To increase the thermal isolation of the leg, one supporting leg is designed in a serpentine shape. In addition, the $\mathrm{SiN}_x$ leg is proposed to be low-temperature $\mathrm{SiN}_x$, which has lower thermal conductivity ($\sim$3 W/(K·m)). The pixel parameters are listed in Table IV. Compared to the parameters in Table II of single-layer cantilevers, the new design greatly improves $S_T, G_{\mathrm{leg}}$ and the thermal response $H$.

As mentioned in the Section II-A, the IR penetration depth in $\mathrm{SiN}_x$ film is about 1 $\mu$m. Since the thickness of $\mathrm{SiN}_x$ layer is assumed to be 0.2 $\mu$m, a large part of the incident IR will penetrate the $\mathrm{SiN}_x$ layer and be reflected by the Au layer. The reflected and incident IR electromagnetic wave will form an interference pattern that would modulate the intensity along the direction normal to the surface as a sinusoidal wave function. Noticing that the intensity at the gold surface reaches the lowest value, and goes to the highest at the quarter-wavelength ($\sim$2.5 $\mu$m for $\lambda_{\mathrm{IR}} = 10$ $\mu$m) position, the $\mathrm{SiN}_x$ layer right next to the reflective surface would not absorb incident IR effectively. To increase the IR absorption in the two-layer pixel design, an additional absorption pad made of 1 $\mu$m $\mathrm{SiN}_x$ is added under the bi-material cantilever with a separation of 2.5 $\mu$m. Besides the absorption pad, an antireflective IR coating on the back side of the Si substrate will reduce the loss of IR influx.

Although we have used a diffractive method for the optical readout, it is unlikely that diffraction can be used for pixel sizes down to 25 $\mu$m. This is because photolithography limits the minimum feature size to about 1 $\mu$m such that the smallest finger periodicity is 4 $\mu$m. Therefore, one cannot accommodate a sufficiently large number of interdigital fingers within 25 $\mu$m. Hence, one must instead use optical interferometry. Interference can be formed between the laser reflected from the gold reflective pad and a reference surface, which is a partially reflective plate that covers the FPA. The resulting interference pattern, which is captured by a CCD camera, follows a formula that is similar to (8) but where $h$ is now the distance between the gold reflective pad and the partially reflective plate. Therefore, the optical detection sensitivity $\beta$ is same as that of the diffraction grating method described above.

To minimize CCD noise in the optical readout system, one wants large number of electrons (large well size) in each CCD pixel. Currently, the maximum CCD well size is about $65 \times 10^4$ electrons. Using this value, the shot-noise limit is: $(\Delta I/I)_{\mathrm{CCD}} = 1/\sqrt{N} = 0.001$. Measurement of the intensity noise of a vertical-cavity surface-emitting laser (VCSEL) indicates that in a bandwidth from 0.1 Hz to 30 Hz, the fluctuations $\Delta I/I < 10^{-4}$ (Fig. 11). For thermal stability, the development of a feedback temperature control system and a thermal package design are in progress to control the FPA chip's temperature to within 50 $\mu$K. The noise analysis and expected NETD for this two-layer design are shown in Table V. It is important to point out that an NETD of approximately 3 to 5 mK seems possible using this technique.

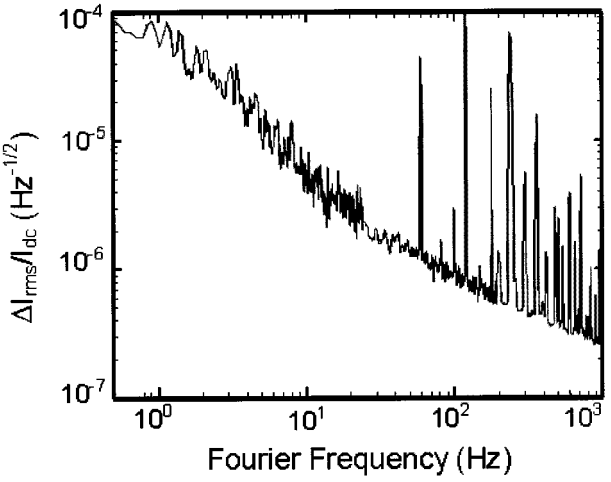


Fig. 11. Noise spectrum of light intensity from a vertical cavity surface wavelength of 800 nm. The relative noise $(\Delta I_{\mathrm{rms}}/(I_{\mathrm{dc}}))$ over a 30-Hz bandwidth is dominated by low-frequency noise and is less than $10^{-4}$.

## VII. CONCLUSION

This paper presents the design concept of an optomechanical uncooled IR imaging system. The focal plane array consisted of a Au/$\mathrm{SiN}_x$ bimaterial microcantilever beam in each pixel, where the beam served both as the IR absorber and the temperature sensor. To thermally isolate each microcantilever from the Si substrate, a serpentine 200 $\mu$m long bare $\mathrm{SiN}_x$ leg was used, which made the leg thermal conductance as low as three times the radiative conductance. Since the thermomechanical response of the cantilever is strongly related to the total length of the bimaterial part, a design of staggered pixel tiling was proposed, which doubled the cantilever length (200 $\mu$m) for the pixel size (100 $\mu$m). The thermal deflection of the cantilever was detected by a visible optical readout system based on Fourier optics and that relied on a deformable grating composed of interdigital fingers fabricated on each cantilever. The

TABLE V
TWO-LAYER FPA DESIGN NOISE ANALYSIS AND NETD

| Pixel size (μm) | $\Delta T_{th}$ (μK) | $\Delta T_{th,vib}$ (μK) | $\Delta T_{CCD}$ (μK) | $\Delta T_{laser}$ (μK) | $\Delta T_{sub}$ (μK) | $\Delta T_{total}$ (μK) | NETD (mK) | $NETD_{TF}$ (mK) |
|---|---|---|---|---|---|---|---|---|
| 25 | 49.8 | 4.8 | 517 | 52 | 50 | 674 | 337 | 24.9 |
| 65 | 60.3 | 8.48 | 71 | 7 | 50 | 197 | 6.6 | 2 |
| 110 | 44.6 | 12.5 | 25 | 2 | 50 | 134 | 2.2 | 0.7 |

thermal image result showed some nonuniformity of the pixel's response, which was due to the nonuniform initial deflection of the cantilever induced by the microfabrication process. The difficulty in stress control in the microfabrication process implied that a compensation strategy in the optical readout system would be necessary.

The estimation of the system NETD based on noise analysis showed that the current system performance is limited by the temperature stability of the feedback control system. With the 20 mK resolution of the control system, the system NETD was calculated to be 1.1 K. However, the thermodynamic temperature fluctuation noise limited $NETD_{TF}$ was calculated to be 1.1 mK. Thus, the system shows potential for much future improvement. The paper also presents a new design with a two-layer cantilever structure for improvement of performance. Analysis shows that with a similar pixel size, the new design increases the thermomechanical response of the cantilever $(S_T)$ to 2.5 $\mu$m/K compared with the 0.11 $\mu$m/K of the one-layer design. Improvement of NETD also depends on better performance of the temperature stability-control system and the visible optical detecting system, which are part of our current research effort. Noise analysis suggests that NETD $\sim 5$ mK can be achieved.

## ACKNOWLEDGMENT

The authors are thankful for the support they received from their program monitors R. Balrerak, E. Towe, C. Hanson, and R. Shimabukuro. T. Perazzo and O. Kwon deserve much credit for the initial work. M. Ray and R. Anderson from SBRC are acknowledged for their contributions in some of the microfabrication. They would also like to thank T. Kenny for useful suggestions.

## REFERENCES

[1] R. G. Buser and M. F. Tompsett, "Uncooled infrared imaging arrays and systems: Historical overview," *Semiconductors Semimetals*, vol. 47, pp. 1–14, 1997.
[2] P. W. Kruse, "Priniple of uncooled infrared focal plane arrays," *Semiconductors Semimetals*, vol. 47, pp. 17–44, 1997.
[3] R. A. Wood, "Uncooled infrared imaging arrays and systems: Monolithic silicon microbolometer arrays," *Semiconductors and Semimetals*, vol. 47, pp. 45–68, 1997.
[4] H. Jeromiek, F. Picard, N. R. Swart, M. Renaud, M. Levesque, M. Lehoux, J. Castonguay, M. Pelletier, G. Bilodeau, D. Audet, T. D. Pope, and P. Lambert, "Micromachined, uncooled $VO_2$ based IR bolometer arrays," in *Proc. SPIE*, vol. 2746, 1996, pp. 60–71.
[5] P. Kruse, R. Dodson, S. Anderson, L. Kantor, M. Knipfer, and T. McManus, "Infrared imager employing a $160 \times 120$ pixel uncooled bolometer array," in *Proc. SPIE*, vol. 3436, 1998, pp. 572–277.
[6] W. A. Radford, D. F. Murphy, A. Finch, A. Kennedy, J. K. Kojiro, M. Ray, R. Wyles, R. Coda, E. A. Moody, and S. Baur, "Microbolometer uncooled infrared camera with 20 mK NETD," in *Proc. SPIE*, vol. 3379, 1998, pp. 22–35.
[7] W. Radford, D. Murphy, A. Finch, K. Hay, A. Kennedy, M. Ray, A. Sayed, J. Wyles, R. Wyles, and J. Varesi, "Sensitivity improvements in uncooled microbolometer FPAs," in *Proc. SPIE*, vol. 3698, 1999, pp. 119–130.
[8] J. K. Gimzewski, Ch. Gerber, E. Meyer, and R. R. Schlittler, "Observation of a chemical reaction using a micromechanical sensor," *Chem. Phys. Lett.*, vol. 217, pp. 589–594, 1994.
[9] J. R. Barnes, S. J. Stephenson, M. E. Welland, Ch. Gerber, and J. K. Gimzewski, "Photothermal spectroscopy with femtojoule sensitive using a micromechanical device," *Nature*, vol. 72, pp. 79–82, 1994.
[10] P. I. Oden, P. G. Datskos, and T. Thundat, "Uncooled thermal imaging using piezoresistive microcantilever," *Appl. Phys. Lett.*, vol. 69, pp. 3277–3279, 1996.
[11] P. G. Dastkos, P. I. Oden, T. Thundat, E. A. Wachter, R. J. Warmack, and S. R. Hunter, "Remote infrared radiation detection using piezoresistive microcantilevers," *Appl. Phys. Lett.*, vol. 69, pp. 2986–2988, 1996.
[12] J. Lai, T. Perazzo, Z. Shi, and A. Majumdar, "Optimization and performance of high-resolution micro-optomechanical thermal sensors," *Sens. Actuators*, vol. 58, pp. 113–119, 1997.
[13] J. Varesi, J. Lai, T. Perazzo, Z. Shi, and A. Majumdar, "Photothermal measurements with picoWatt resolution using micro-optomechanical sensors," *Appl. Phys. Lett.*, vol. 71, pp. 306–308, 1997.
[14] P. Norton, M. Mao, T. Perazzo, Y. Zhao, O. Kwon, A. Majumdar, and J. Varesi, "Micro-optomechanical infrared receiver with optical readout-MIRROR," in *Proc. SPIE*, vol. 4028, Orlando, FL, Apr. 2000.
[15] S. R. Manalis, S. C. Minne, C. F. Quate, G. G. Yaralioglu, and A. Atalar, "Two-dimensional micromechanical bimorph arrrays for detection of thermal radiation," *Appl. Phys. Lett.*, vol. 70, pp. 3311–3313, 1997.
[16] M. Mao, T. Perazzo, O. Kwon, and A. Majumdar, "Infrared vision using an uncooled thermo-opto-mechanicsl camera: Design, microfabrication, and performance," *Proc. IEEE MEMS Conf.*, pp. 100–105, Jan. 17–21, 1999.
[17] T. Perazzo, M. Mao, O. Kwon, and A. Majumdar, "Infrared vision uncooled micro-optomechanical camera," *Appl. Phys. Lett.*, vol. 74, pp. 3567–3569, 1999.
[18] S. M. Lee and D. G. Cahill, "Heat transport in thin dielectric films," *J. Appl. Phys.*, vol. 81, pp. 2590–2595, 1997.
[19] D. Sarid, *Scanning Force Microscopy*. New York: Oxford University Press, 1991.
[20] J. W. Goodman, *Introduction to Fourier Optics*: McGraw-Hill, 1968.
[21] M. Born and E. Wolf, *Principles of Optics*. NewYork: Pergamon, 1959.
[22] Y. Zhao, M. Mao, and A. Majumdar, "Application of Fourier optics for detecting deflection of infrared-sensing microcantilever arrays," *Microscale Thermophys. Eng.*, vol. 3, pp. 249–251, 1999.
[23] P. J. French, P. M. Sarro, R. Mallée, E. J. M. Fakkeldij, and R. F. Wolffenbuttel, "Optimization of a low-stress silicon nitride process for surface-micromachining applications," *Sens. Actuators*, vol. 58, pp. 149–157, 1997.

**Yang Zhao** received the B.S. and M.S. degrees in mechanical engineering from University of Science and Technology of China (USTC), Hefei, China, in 1994 and 1997, respectively. She is currently working towards the Ph.D. degree in mechanical engineering at University of California, Berkeley.

Her research interests include design and fabrication of MEMS and optical detection technique.

**Minyao Mao** received the B.S. degree in physics from Fudan University, China, in 1989 and the Ph.D. degree from Shanghai Institute of Metallurgy, Chinese Academy of Science, China, in 1994.

From 1995 to 1997, he was a Postdoctoral Fellow in Lawrence Berkeley National Laboratory and Department of Physics, University of California at Berkeley. From 1998 to 1999, he was a Postdoctoral Researcher in the Department of Mechanical Engineering, University of California, Berkeley. From 2000 to 2001, he was a Senior Scientist/Engineer in JDSU, Santa Rosa, CA. He is currently a principle MEMS engineer in a MEMS startup. His main research interest is developing MEMS engines for various fiber optical products in telecommunication field.

**Roberto Horowitz** received the B.S. degree with highest honors in mechanical engineering and the Ph.D. degree from the University of California, Berkeley, in 1978 and 1983, respectively.

He is currently a Professor and the Vice-Chairman of graduate study in the Department of Mechanical Engineering, University of California, Berkeley. He is teaching and conducting research in the areas of adaptive, learning, nonlinear and optimal control and mechatronics, with applications to disk file systems, robotics, microelectromechanical systems (MEMS's), and intelligent vehicle and highway systems (IVHS's).

Dr. Horowitz was the recipient of a 1984 IBM Young Faculty Development Award and a 1987 National Science Foundation Presidential Young Investigator Award.

**Arunava Majumdar** received the B.Tech degree in mechanical engineering from the Indian Institute of Technology, Bombay, India, in 1985 and the Ph.D. degree in mechanical engineering from University of California, Berkeley, in1989.

He is currently a Professor and the Vice-Chairman of Instructions in the Department of Mechanical Engineering, University of California, Berkeley. Previously, he was with the Arizona State University, Tempe, from 1989 to 1992 and the University of California, Santa Barbara (from 1992 to 1996 as a faculty member in mechanical engineering. His research interests in his group range from MEMS, micro/nanoscale thermophysics to nanobiomolecular engineering and nanoscale imaging. He is currently serving as an Associate Editor for the A*SME Journal of Heat Transfer* and the I*nternational Journal of Heat and Mass Transfer*, and is Co-Editor-in-Chief of *Microscale Thermophysical Engineering*.

Dr. Majumdar is a recipient of the NSF Young Investigator Award, the ASME Melville Medal, and the ASME Best Paper Award from the Heat Transfer Division. He also serves as a member of the Council on Energy Engineering Research for the Department of Energy and the ASME Steering Committee on Nanotechnology.

**John Varesi** received the B.S. degree in mechanical engineering from the University of California, Los Angeles (UCLA) and the M.S. degree in mechanical engineering with emphases in thermal science from the University of California, Santa Barbara, in 1995 and 1997, repectively. His thesis work involved the development and implementation of a microscale temperature measurement system and technique. He also performed preliminary studies examining the feasibility of a micromechanical infrared sensor.

Currently, he is with Raytheon Infrared Operations, Goleta, CA. Initially, he spent two years assisting in the development of infrared microbolometers. At the present time, he is primarily focused on advanced focal-plane-array development using HgCdTe photovoltaic infrared detectors.

**Paul Norton** received the A.B. degree in physics from Carleton College, Northfield, MN, in 1965 and the Ph.D. degree in solid state physics from Syracuse University, Syracuse, NY, in 1970. He scored in the 94th percentile on physics GRE.

He was a William E. Carleton scholarship recipient and from 1965 to 1966, he was a Teaching Assistant and from 1966 to 1970, he was a Research Assistant. He is currently consulting part time for the U.S. Army Night Vision and Electronic Sensors Directorate, Fort Belvoir, VA; the Ballistic Missile Defense Organization, and for an uncooled IR detector program at UC Berkeley.

**J. Kitching**, photograph and biography not available at the time of publication.